CHAOS 2448
7 March 2003 Disk used
ARTICLE IN PRESS
No. of Pages 10, DTD = 4.3.1
SPS-N, Chennai

Available online at www.sciencedirect.com
SCIENCE DIRECT®

CHAOS
SOLITONS & FRACTALS

PERGAMON
Chaos, Solitons and Fractals xxx (2003) xxx–xxx
www.elsevier.com/locate/chaos

Multi-fractal thermal characteristics of the southwestern GIN sea upper layer

Peter C. Chu

Naval Ocean Analysis and Prediction Laboratory, Department of Oceanography, Naval Postgraduate School, Monterey, CA 93943, USA

Accepted 19 February 2003

1. Introduction

The Greenland Sea, Iceland Sea, and Norwegian Sea (GIN Sea) are key regions in the advective–convective system with various stages of modification that links the polar ocean with the North Atlantic (Fig. 1). Because of the import and modification of water masses a large number of regional water types can be encountered. The North Atlantic Water (NAW) is relatively warmer and saline ($T > 2$ °C, $S > 34.9$ ppt). The Arctic Water (AW) is cooler and fresher ($T < 0$ °C, $S < 34.7$ ppt) [1]. Different water masses encountered in the GIN Sea interface and form fronts and eddies that not only determine water bodies with different hydrographic characteristics but also the regional biological systems. The major circulation pattern of the GIN Sea is characterized by the Northward flowing Norwegian Atlantic Current (NAC) in the east and the southwestward flowing East Greenland Current (EGC) along the East Greenland shelf and leaving the Iceland Sea via the Denmark Strait.

Convection in GIN Sea is seen as a globally important process in which air–sea interactions influence oceanic circulation through the production and ventilation of deep and intermediate waters. The key dynamic elements of oceanic convection are taken to be the individual plumes, clusters of plumes or called chimneys, and eddies that are the consequence of chimneys aging in a rotating frame. Two major features, nonstationarity and intermittency, should be first investigated in order to understand oceanic convective process or the secondary circulation across oceanic fronts [2]. Question arises: How can we determine upper ocean nonstationarity and intermittency from observational data? This paper describes a multi-fractal analysis on a high-resolution temperature dataset to obtain the nonstationarity and intermittency of the upper layer (300 m depth) in the southwestern GIN Sea.

2. Thermistor chain data

In July–August 1987, fine-resolution temperature data are collected on board of M/V SEA SEACHER by the Royal Navy's Admiralty Research Establishment (ARE) using a digital thermistor chain (280 m long, 100 sensor pods) with a single 200 km straight-line tow (4 knots speed) near 69 °N, 18 °W (Fig. 2) in the east edge of EGC [3]. The upper ocean (surface to 280 m depth) was sampled every 0.9 s, obtaining a temperature profile about every 2 m along the track. Each sensor pod of the chain measures temperature, and about one in five also measures pressure, allowing the depth distribution of temperature to be deduced.

Fig. 3 shows contour plot of temperature ranging from 2 to 8 °C with 0.2 °C increment on a vertical cross-section between the two marked locations '*b*' and '*e*' (Fig. 2). As pointed by Scott and Killworth [3], the temperature shows a small-scale variability with highly irregular nature. The total length of the temperature cross-section is 90 km with each interval of 6 km. The thin surface layer (depth around 5 m) temperature is about +7.5 °C. Below the surface layer, there is a first thermocline with temperature rapidly decreasing with depth to 25 m. The vertical gradient in the first thermocline is very strong (~0.45 °C/m). Cold, relatively uniform sublayer exists below the first thermocline from 25 to 70 m, reaching a minimum temperature of −1.5 °C. Below the cold sublayer, there is a second thermocline (70–90 m, thickness around 20 m) where the temperature increases with depth with a vertical temperature gradient around 0.135 °C/m. Below the second thermocline, there exists a warm intermediate layer (~100–300 m) with a maximum temper-

0960-0779/03/$ - see front matter
doi:10.1016/S0960-0779(03)00041-9

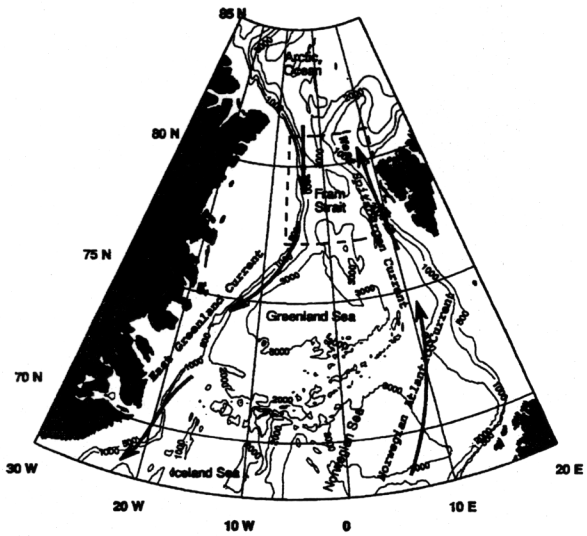

Fig. 1. Schematic representation of bathymetry and currents in the GIN Sea.

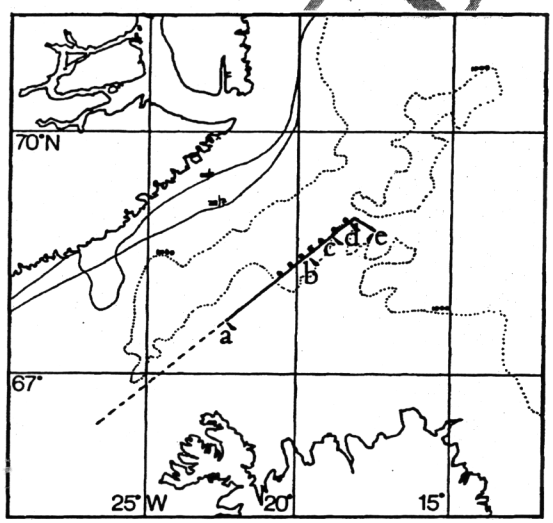

Fig. 2. Track along which the thermistor chain data were taken. The dotted curve represents 1000 m depth contour (after Scott and Killworth [3]).

ature of +1.2 °C. Note that the thermal characteristics are different between the two thermoclines. The first (second) thermocline features the decrease (increases) of temperature with depth. The chimneys are observed below the characteristic cold sublayer (70 m depth) with width of 3 km (Fig. 4). The water is about 1.2 °C cooler within than out of the chimneys. The chimneys reach the maximum thermistor chain depth (~280 m). Containing water of temperature down to about 0 °C, the chimneys appear to punch the cold water clearly through the warm intermediate layer water with a maximum temperature of +1.2 °C.

3. Power spectra

What is the inherent thermal variability identified from this high-resolution temperature data with multi-layer and chimney structures? What are the statistical properties? Before answering these questions, we should first investigate the

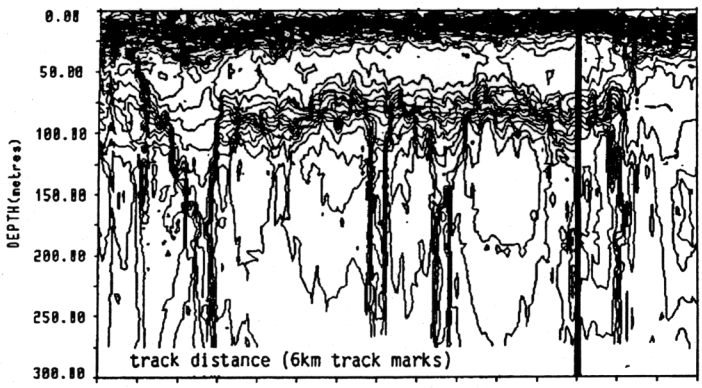

Fig. 3. Temperature cross-section obtained from the thermistor chain data collected along the track from Station-b to Station-e (after Scott and Killworth [3]).

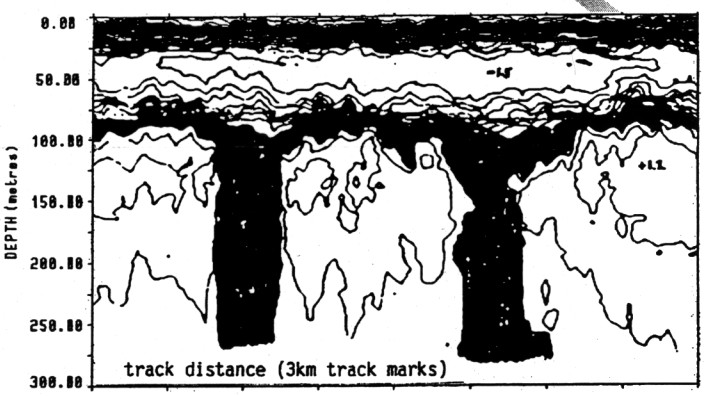

Fig. 4. An expansion of central part of Fig. 3 showing 30 km section between Station-c and Station-d (after Scott and Killworth [3]).

stationarity of the temperature field. For a given depth, the temperature data is a function of the horizontal coordinates, x,

$$T_i = T(x_i), \quad x_i = il, \quad i = 0, 1, \ldots, \Lambda, \quad \Lambda = L/l, \tag{1}$$

where $l = 2$ m, is the horizontal resolution of the data, and L is the total horizontal scale of the data set. Our data set has 24,000 temperature profiles, that is, $\Lambda = 45{,}000$.

Spectral analyses of temperature field,

$$E_j = E(k_j), \quad k_j = j/L, \quad j = 1, 2, \ldots, \Lambda/2. \tag{2}$$

at all depths were done, but for the sake of brevity and to elucidate the important points, only spectrum at 20 m depth (cold sublayer, Fig. 5) is shown. A Bartlett window was used to taper the ends of each series before calculating the power spectra to reduce the spectral leakage in the wavenumber domain. Fig. 5 shows the existence of a spike on

$$\log_2(kL/2) \simeq 6.5,$$

corresponding to a scale of approximate 3 km in the thermal variability. This length scale (3 km) coincides with the chimney scale, which may imply the existence of a linkage between the cold sublayer and the chimney formation.

4. Stationarity

For a scaling process, one expects power law behavior [4],

$$E(k) \propto k^{-\beta}, \tag{3}$$

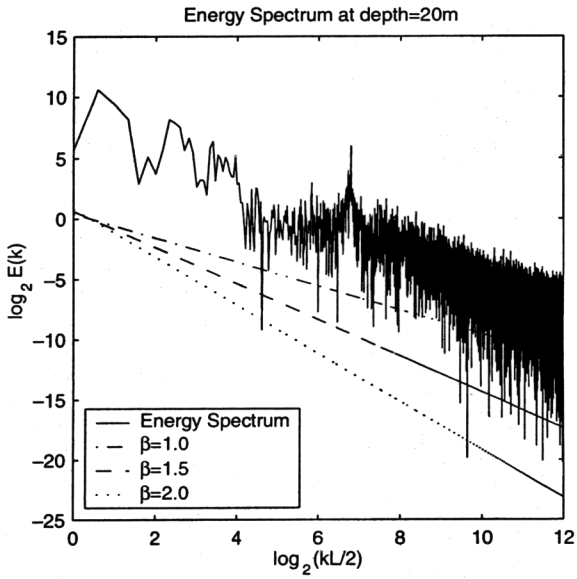

Fig. 5. Power spectrum of temperature filed at 20 m depth.

over a large range of wavenumber k. The spectral exponent β contains information about the degree of stationarity of the data [5,6]. If $\beta < 1$, the field is stationary; if $1 < \beta < 3$, the field contains nonstationary signal with stationary increments and in particular, the small-scale gradient field is stationary; if $\beta > 3$, the field is nonstationary with nonstationary increments.

The power spectra for all the depths have multi-scale characteristics with the spectral exponent β in the range of

$$1 < \beta < 2, \tag{4}$$

which means the temperature field of the southwestern GIN Sea sublayer is nonstationary with stationary increments (Fig. 5).

5. Structure functions

Since the thermistor chain data set has stationary increments, we should study the statistical characteristics of the gradient field,

$$|\Delta T(r;x)| = |T(x_{i+r}) - T(x_i)|, \quad i = 0, 1, \ldots, \Lambda - r, \tag{5}$$

where r denotes the lag between two data points. Obviously, r is inversely proportional to the wavenumber k,

$$r \propto \frac{1}{k}.$$

Structure functions are used to depict the thermal variability. The qth-order structure function is defined by the mean of the qth power of the gradient field $|\Delta T(r;x)|$,

$$S(r,q) \equiv \langle |\Delta T(r;x)|^q \rangle = \frac{1}{\Lambda - r} \sum_{i=0}^{\Lambda - r} |\Delta T(r;x)|^q. \tag{6}$$

For example, $r = 1$, $q = 1$, the structure function

$$S(1,1) = \frac{1}{\Lambda - 1} \sum_{i=0}^{\Lambda - 1} |T(x_{i+1}) - T(x_i)|, \tag{7}$$

represents the average magnitude of gradient.

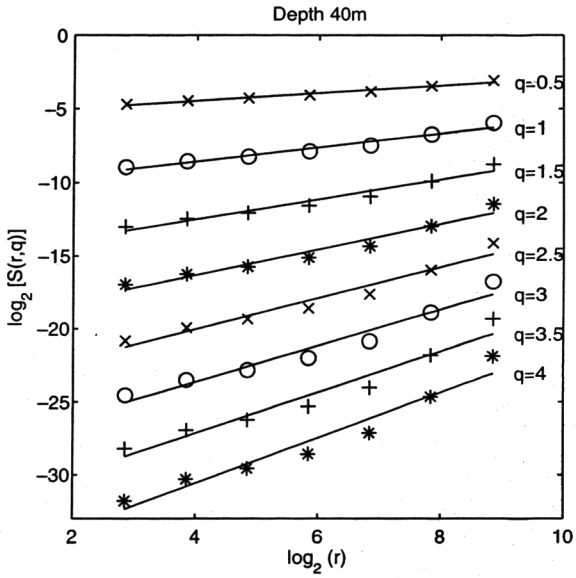

Fig. 6. Structure functions for different q-values (depth = 40 m).

Near-linear dependence of $\log_2[S(r,q)]$ on $\log_2(r)$ is found with different q-values from 0.5 to 4.0 (Fig. 6). The straight lines with different slopes show that the structure functions for the upper ocean temperature in the southwestern GIN Sea satisfies the power law

$$S(r,q) \propto r^{\zeta(q)}, \tag{8}$$

with the exponent $\zeta(q)$ depending on q. Since $S(r,0) = 1$, the power $\zeta(q)$ should be 0 for $q = 0$. Our computation (Fig. 6) agrees quite well with earlier studies [7,8]. $\zeta(q)$ is monotonically and near-linearly increasing with q. Thus, it may be represented by

$$\zeta(q) = H(q)q, \tag{9}$$

where $H(q)$ is nearly a constant.

The power of the structure function, $\zeta(q)$, is computed for the whole dataset. Fig. 7 shows the dependence of $\zeta(q)$ on q for selected levels. All the curves (near-linear) converges at $q = 0$ [$\zeta(0) = 0$], and show three different patterns: (a) slow increasing with q (surface layer, 0 m), (b) intermediate-rate increasing with q (second thermocline, 80 m), (c) fast increasing with q (first thermocline, 20 m; cold sublayer, 40–60 m; intermediate warm layer, below 100 m).

The structure function for $q = 1$, $S(r,1)$, is often used to determine the statistical characteristics of the data such as stochastically continuous and stationarity. When the structure function $S(r,1)$ does not depend on r

$$S(r,1) = \text{const}, \tag{10}$$

which denotes exact stationary. Eq. (10) is equivalent to

$$\zeta(1) = H(1) = 0.$$

Thus, $H_1 \equiv H(1)$, represents statistical characteristics of data. Since the power $\zeta(1)$ (i.e., $H(1)$) varies with depth (Table 1) between 0.11 at the surface and 0.56 at 120 m depth (intermediate warm layer), the thermal field in the southwestern GIN Sea is nearly stationary.

If $g(T)$ is defined as the graph of $T(x)$, whose dimension can be defined by [9]

$$D_{g(T)} = 2 - H_1. \tag{11}$$

For a stochastically continuous ($H_1 = 1$) data $T(x)$, the graph should be a smooth curve, whose dimension, $D_g(T)$ should be 1. If the graphs $g(T)$ fill the whole space (exact stationary),

$$D_{g(T)} = 2, \tag{12}$$

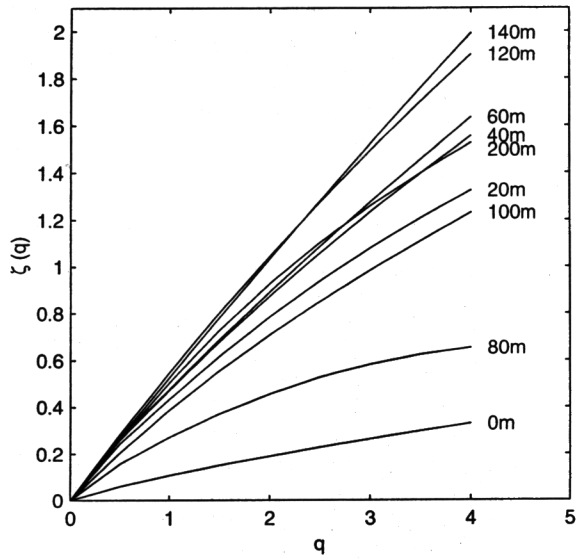

Fig. 7. Dependence of the structure function's power, $\zeta(q)$, on q and depth.

Table 1
Power of the structure function $S(r,1)$ and the dimension of the GIN Sea thermal field T

Depth (m)	0	20	40	60	80	100	120	140	200
$\zeta(1) = H_1$	0.11	0.43	0.47	0.48	0.28	0.40	0.56	0.52	0.50
$D_{g(T)}$	1.89	1.57	1.53	1.52	1.78	1.60	1.44	1.48	1.50

which corresponds to $H_1 = 0$.

Table 1 shows that the dimension of the southwestern GIN Sea upper thermal field varies (multi-dimension structure) from higher values such as 1.89 (surface: 0 m), 1.78 (second thermocline: 80 m) to lower values such as 1.57 (first thermocline: 20 m), 1.52–1.53 (cold sublayer: 40, 60 m), and 1.44–1.50 (warm intermediate layer: 120, 140, 200 m). The decreasing order of stationarity is: ocean surface, second thermocline, first thermocline, cold sublayer, and warm intermediate layer.

6. Singular measures

Normalized small scale absolute gradient

$$\varepsilon(1;x_i) = \frac{|\Delta T(1;x_i)|}{\langle|\Delta T(1;x_i)|\rangle}, \quad \langle|\Delta T(1;x_i)|\rangle = \frac{1}{\Lambda}\sum_{i=0}^{\Lambda-1}|\Delta T(1;x_i)|, \tag{13}$$

is used to identify the intermittency of the thermal field. The running average of r normalized values are computed by

$$\varepsilon(r;x_i) = \frac{1}{r}\sum_{j=i}^{i+r-1}\varepsilon(1;x_j), \quad i = 0,1,\ldots,\Lambda - r. \tag{14}$$

The mean of the qth power of $\varepsilon(r;x_i)$

$$M(r,q) \equiv \langle\varepsilon(r;x_i)^q\rangle = \frac{1}{\Lambda - r}\sum_{i=0}^{\Lambda-r}[\varepsilon(r;x_i)]^q, \tag{15}$$

is defined as the qth-order singular measure. Obviously, for $q = 0$,

$$M(r,0) = 1. \tag{16}$$

For $q = 1$,

$$M(r,1) \equiv \langle \varepsilon(r;x_i) \rangle = \frac{1}{\Lambda - r} \sum_{i=0}^{\Lambda - r} [\varepsilon(r;x_i)] = \frac{1}{\Lambda - r} \sum_{i=0}^{\Lambda - r} \left[\frac{1}{r} \sum_{j=i}^{i+r-1} \varepsilon(1;x_j) \right] = 1. \tag{17}$$

The singular measures are computed for all depths. For simplicity, $M(r,q)$ for the depth of 40 m is given here (Fig. 8). Near-linear dependence of $\log_2[M(r,q)]$ on $\log_2(r)$ is found with different q-values from 0.5 to 4.0. The straight lines with different slopes show that the singular measures with various q for the upper layer temperature in the southwestern GIN Sea satisfies the power law

$$M(r,q) \propto r^{-K(q)}, \quad q \geqslant 0, \tag{18}$$

with the power $K(q)$ varying with q. From Eqs. (16) and (17), we have

$$K(0) = K(1) = 0. \tag{19}$$

Several characteristics are found from Fig. 9: The power $K(q)$ is a convex function

$$\frac{\mathrm{d}^2 K(q)}{\mathrm{d}q^2} > 0, \tag{20}$$

for all q and

$$K(q) < 0 \quad \text{only if } 0 < q < 1 \tag{21}$$

which reflects the fact that, in this range, taking a qth power necessarily reduces the fluctuation of $\varepsilon(r;x_i)$; and otherwise

$$K(q) \geqslant 0, \quad \text{if } q \geqslant 0. \tag{22}$$

Following [10,11] we may define a function

$$C(q) = \frac{K(q)}{q-1}. \tag{23}$$

For $q \to 1$, we use *l'Hosptal*'s rule to define a straightforward measure of inhomogeneity in the sense of singular measure [4]:

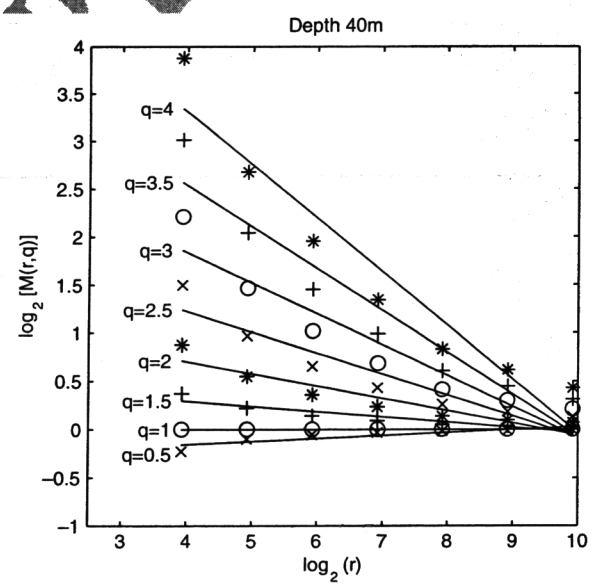

Fig. 8. Singular measures for different q-values (depth = 40 m).

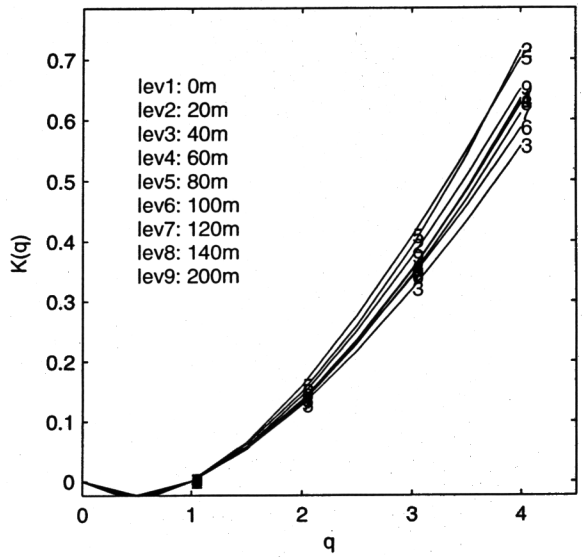

Fig. 9. Dependence of the singular measure's power, $K(q)$, on q and depth.

$$C_1 \equiv C(1) = K'(1) \geqslant 0, \tag{24}$$

which is called the intermittency parameter. The larger the value of C_1 the lager the intermittency and singularity the data set has. The intermittency parameter C_1 varies from 0.08 to 0.1.

7. Mean multi-fractal plane

Statistical moments of all orders (qth power) can be computed, however, the first moment ($q = 1$) provides important information about the data. The parameter C_1 measures the degree of intermittency in the system, while H_1 measures its degree of nonstationarity. The plot of C_1 versus H_1 called the mean multi-fractal plane, shows the degree of nonstaionarity and intermittency (Fig. 10).

Both parameters have geometrical interpretations as co-dimensions: information dimension and graph dimension [4]. The information dimension, represented by $(1 - C_1)$, is a first-order estimate of sparseness of strong gradient

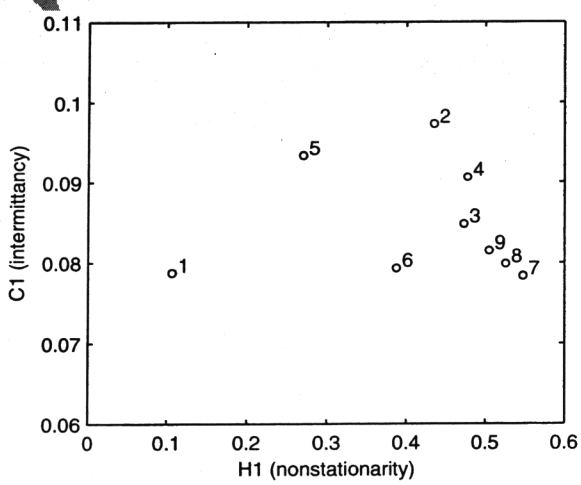

Fig. 10. Mean multi-fractal plane (H_1, C_1) for the southwestern GIN Sea thermal field.

distributed in the system. The graph dimension, represented by $(2 - H_1)$, is a first-order estimate of roughness in the system. Both parameters have analytical meanings: C_1 (sparseness) is related to singularity and H_1 (roughness) is connected to the lack of differentiability. The southwestern GIN Sea upper layer thermal field shows multi-fractal characteristics (Fig. 10) in terms of C_1 and H_1 We find larger variation in H_1 (0.11–0.56) than in C_1 (0.08–0.10). Identification of (H_1, C_1) ranges helps to select realistic model to describe the field [4].

8. Conclusions

The multi-fractal analysis provides a useful framework for analyzing ocean data when complex nonlinear processes. The upper layer thermal structure in the southwestern GIN Sea has the following features:

(1) The energy spectrum at 20 m depth (cold sublayer) shows the existence of a spike at the scale of approximate 3 km in the thermal variability. This length scale (3 km) coincides with the chimney scale, which may imply the existence of a linkage between the cold sublayer and the chimney formation.
(2) The power spectra for all the depths have multi-scale characteristics with the spectral exponent β in the range of (1, 2). This means the temperature field of the southwestern GIN Sea sublayer is nonstationary with stationary increments.
(3) The structure function has multi-fractal characteristics, i.e., the power of the qth-order structure function is monotonically and near-linearly increasing with q. However, the rate of such an increasing varies with depth: (a) slow increasing with q (surface layer, 0 m), (b) intermediate-rate increasing with q (second thermocline, 80 m), (c) fast increasing with q (first thermocline, 20 m; cold sublayer, 40–60 m; intermediate warm layer, below 100 m).
(4) Two parameters for the first moment ($q = 1$) structure function and sigular measure, H_1 and C_1 are important to represent the multi-fractal characteristics in terms of co-dimensions (information and graph). The graph dimension, represented by $(2 - H_1)$, is a first-order estimate of roughness in the system. The information dimension, represented by $(1 - C_1)$, is a first-order estimate of sparseness of strong gradient distributed in the system. Both parameters have analytical meanings: C_1 (sparseness) is related to singularity and H_1 (roughness) is connected to the lack of differentiability.

The graph dimension of the southwestern GIN Sea upper thermal field varies (multi-dimension structure) from higher values such as 1.89 (surface: 0 m), 1.78 (second thermocline: 80 m) to lower values such as 1.57 (first thermocline: 20 m), 1.52–1.53 (cold sublayer: 40, 60 m), and 1.44–1.50 (warm intermediate layer: 120, 140, 200 m). The decreasing order of the stationarity is: the ocean surface, second thermocline, first thermocline, cold sublayer, and warm intermediate layer. However, the information dimension of the southwestern GIN Sea upper thermal field varies slightly from 0.92 to 0.90. This indicates that singularity is very low.

Acknowledgements

The author wish to thank John Scott at ARE of the Royal Navy for most kindly providing the thermistor chain data and Laura Ehret and Chenwu Fan at the Naval Postgraduate School for computational assistance. This work was funded by the Office of Naval Research and the Naval Postgraduate School.

References

[1] van Aken HM, Quadfasel D, Warpakowski A. The Arctic front in the Greenland Sea during February 1989: Hydrographic and biological observations. J Geophys Res 1991;96:4739–50.
[2] Chu PC. C-Vector for identification of oceanic secondary circulations across arctic fronts in fram strait. Geophys. Res. Lett., in press.
[3] Scott JC, Killworth PD. Upper ocean structures in the southwestern Iceland Sea—a preliminary report. In: Chu PC, Gascard JC, editors. Deep convection and deep water formation in the oceans, vol. 57. Elsevier Oceanographic Series; 1991. p. 107–21.
[4] Davis A, Marshak A, Wiscombe W, Cahalan R. Multifractal characteristics of nonstationarity and intermittency in geophysical fields: Observed, retrieved, or simulated. J Geophys Res 1994;99:8055–72.
[5] Mandelbrot BB. The fractal geometry of nature. New York: W.H. Freeman; 1982. p. 460.

[6] Schertzer D, Lovejoy S. Physical modeling and analysis of rain clouds by anisotropical scaling multiplicative processes. J Geophys Res 1987;92:9693–714.
[7] Frisch U. From global scaling a la Kolmogorov, to local multifractal in fully developed turbulence. Proc Roy Soc Lon 1991;A434:89–99.
[8] Marshak A, Davis A, Cahalan R, Wiscombe W. Boundary cascade models as non-stationary multifractals. Phys Rev E 1994;49:55–69.
[9] Mandelbrot BB. Fractals: form chance and dimension. New York: W.H. Freeman; 1977. 365 pp.
[10] Grassberger P. Generalized dimensions of strange attractors. Phys Rev Lett A 1983;97:227–330.
[11] Hentschel HGE, Procaccia I. The infinite number of generalized dimensions of fractals and strange attractors. Physica D 1983;8:435–44.